Effects of Temperature Distributions on Thermally Induced Behavior of UHPC Shear Key Connections of an Adjacent Precast Prestressed Concrete Box Beam Bridge

Ali A. Semendary, A.M.ASCE[1]; Eric P. Steinberg, Ph.D., P.E.[2]; Kenneth K. Walsh, Ph.D.[3]; and Elné Barnard, S.M.ASCE[4]

Downloaded from ascelibrary.org by Iowa State University on 01/28/19. Copyright ASCE. For personal use only; all rights reserved.

Abstract: Recently, there has been a rapid increase in using ultrahigh-performance concrete (UHPC) in bridge connections due to its high compressive strength, pre- and postcracking tensile strengths, superior bond, and durability characteristics. However, the behavior of field-cast UHPC connections under temperature effects is not yet fully understood. Furthermore, the temperature distribution that produces the largest thermally induced stresses in UHPC connections is unknown. In this study, the thermally induced stresses in field-cast UHPC shear key connections in an adjacent precast prestressed concrete box beam bridge were investigated using field data as well as a three-dimensional finite-element (FE) model. The FE model was validated using field data and exhibited the ability to capture the behavior of the bridge. A new temperature distribution was noticed based on the data analysis. This temperature distribution has not yet been considered by professional bridge design specifications, although it produced the largest thermally induced stresses in UHPC connections and at the beam–key interface. The observed temperature distribution should be considered in the design of UHPC shear keys for these types of bridges. **DOI: 10.1061/(ASCE)BE.1943-5592.0001346.** *© 2018 American Society of Civil Engineers.*

Author keywords: Temperature; Thermal stress; Finite-element (FE) model; Adjacent box beam; Shear key connection; Ultrahigh-performance concrete (UHPC).

Introduction

Temperature effects on the behavior of bridges are classified into uniform temperature change and temperature gradient. The uniform temperature refers to the average change in temperature over the beam cross section, and it induces either expansion or contraction. When the expansion or contraction is restrained, especially in statically indeterminate structures, thermal forces will develop. The uniform temperature change is normally used to determine the thermal movement in the bridge's design, although the bridge may exhibit nonuniform temperature change. The uniform change in temperature can be calculated using either Procedure A or B based on the type of bridge (AASHTO 2016). The linear or nonlinear temperature changes over the height of the beam refer to the temperature gradient. The linear temperature gradient causes secondary moment when the structure is restrained to prevent the curvature. The nonlinear temperature distribution over the height of the beam causes bending, deflections, and self-equilibrating stresses (Potgieter and Gamble 1983; Imbsen et al. 1985; Hedegaard et al. 2013; Kong et al. 2014; Rodriguez et al. 2014). When the temperatures in the top and the bottom flanges are higher than the temperature in the web, positive temperature gradient will develop. Negative temperature gradient develops when the temperatures in the top and the bottom flanges are lower than the temperature in the web (Potgieter and Gamble 1983; Mahama et al. 2009). In AASHTO (2016) Article 3.12.3, the United States is divided into four zones depending on solar radiation. The specifications consider only the bilinear positive and negative temperature gradients. The positive temperature gradient assumes the temperatures in the top and the bottom flanges are higher than the temperature in the web, whereas the negative temperature gradient assumes the temperatures in the top and bottom flanges are lower than the temperature in the web.

Temperature effects on the behavior of the adjacent precast concrete box beam bridges utilizing regular grouted shear keys have been investigated by many researchers. In the study by Grace et al. (2012), the temperature gradient of a composite adjacent box beam bridge 15 m (50 ft) long was monitored using thermocouples distributed over the bridge depth. The data were compared with AASHTO (2004) and correlated well, and therefore, the temperature gradient from AASHTO (2004) was used in a finite-element (FE) model. The composite box beam bridge exhibited cracks at some locations in the corners of the deck near the barriers as well as at the beam-deck corners. The FE model indicated that the positive temperature gradient caused a tendency of the box beams to separate from each other. This separation created high tensile stresses at the bottom of the deck, which caused the cracks. The FE model used by the authors was not calibrated under temperature changes using field data. FE modeling was also conducting by Dong (2002) to investigate the thermal behavior of a full-scale bridge model, which was tested by Miller et al. (1999), under a uniform temperature and linear temperature gradient of 17°C (30°F). The full-scale bridge model consisted of four box beams connected together by

[1]Ph.D. Candidate, Dept. of Civil Engineering, Ohio Univ., Athens, OH 45701 (corresponding author). ORCID: https://orcid.org/0000-0003-0057-4752. Email: as295111@ohio.edu

[2]Professor, Dept. of Civil Engineering, Ohio Univ., Athens, OH 45701. Email: steinber@ohio.edu

[3]Associate Professor, Dept. of Civil Engineering, Ohio Univ., Athens, OH 45701. Email: walshk@ohio.edu

[4]Graduate Research Assistant, Dept. of Civil Engineering, Ohio Univ., Athens, OH 45701. Email: eb459616@hio.edu

Note. This manuscript was submitted on September 28, 2017; approved on August 7, 2018; published online on November 28, 2018. Discussion period open until April 28, 2019; separate discussions must be submitted for individual papers. This paper is part of the ***Journal of Bridge Engineering***, © ASCE, ISSN 1084-0702.

nonshrink grout in the shear keys. Based on the FE model results, the cracking in the partial-depth shear keys, filled with nonshrink grout, was observed under an upper uniform temperature of 24°C (75°F) and lower uniform temperature of –73°C (–100°F) by assuming a reference temperature of –18°C (0°F). When the temperature gradient was used, the cracks were observed in partial-depth shear keys near the support of shear key connections. However, this observation was based on the behavior only because no strain data were compared to verify the FE model.

Ultrahigh-performance concrete (UHPC) is a new, advanced, cementitious-based composite material that has a low water:cement ratio and high tensile as well as compressive strengths compared to normal or high-strength concrete (Yuan and Graybeal 2014). UHPC has been used as grout material in the state of New York (Perry and Royce 2010). Prototype high-performance concrete (HPC) panels were connected by a joint filled with UHPC material. The joint between a pair of HPC precast deck panels showed no leaking or degradation after applying a million cycles of wheel loadings. Royce (2016) documented using UHPC in New York between prefabricated bridge elements, such as deck bulb tees, transverse and longitudinal joints in full-depth deck panels, and link slab. According to the author, the UHPC joints between prefabricated bridge elements performed well. One application of UHPC for bridge connections was in the shear keys between adjacent box beams (Yuan and Graybeal 2016). A temperature gradient of 28°C (50°F) was created by pumping steam through the top flanges of the box beams. The authors reported that the temperature did not cause any cracks in the UHPC connection or debonding at the beam–shear key interface based on visual inspection.

UHPC has also been used in deck panels as well as longitudinal and transverse connections in a single-span bridge in Wapello County, Iowa. The bridge was prefabricated using full-depth UHPC waffle deck panels installed on five standard Iowa girders. The bridge utilized three types of UHPC connections. The precast UHPC deck panel was connected to the girders by extending the shear hook into shear pocket connections. The center girder and the deck panels were connected by utilizing a shear hook, dowel bar extending from both sides of the connection, as well as longitudinal reinforcement along the total length of the girder. The panel-to-panel connection consisted of reinforcement extending from both sides of the panels with additional transverse reinforcement. The bridge was tested under truck load and performed well (Aaleti et al. 2014). However, cracks were observed, in all types of UHPC connections, either in the joints or at the interface, as presented in Fig. 1. Cracks in UHPC connections were also documented in the study by Phares et al. (2013). The study was conducted on a three-span-wide steel/precast modular structure. The Keg Creek Bridge consists of two 20.5-m (67.3-ft) end spans with a 21.3-m (70-ft) center span. The cross section of the bridge was made up of six precast deck modules. Each module was compositely constructed through the use of shear studs with two steel beams supporting a 216-mm (8.5-in.) concrete deck. Modules were connected on site through the utilization of full-depth longitudinal and transverse moment-resisting joints infilled with UHPC. The bridge was instrumented and tested soon after construction and 7 months later. The heavily instrumented area was in the transverse UHPC connections over the piers because this area is subjected to the negative moment. The bridge performed well after construction when it was tested with different truck-load configurations. However, the results from the truck-load test conducted 7 months later indicated that the strain across the interface between the deck panel and UHPC transverse joint increased significantly because of loss of the bond at the interface. The interface debonding was also confirmed by visual inspection, as presented in Fig. 2. The compressive strain in the bottom flange of the girder at the piers was also significantly reduced because of the reduction in negative moment continuity due to cracks at the interface. The observed cracks indicated that more research on the temperature effects on the behavior of field-cast UHPC connections is needed.

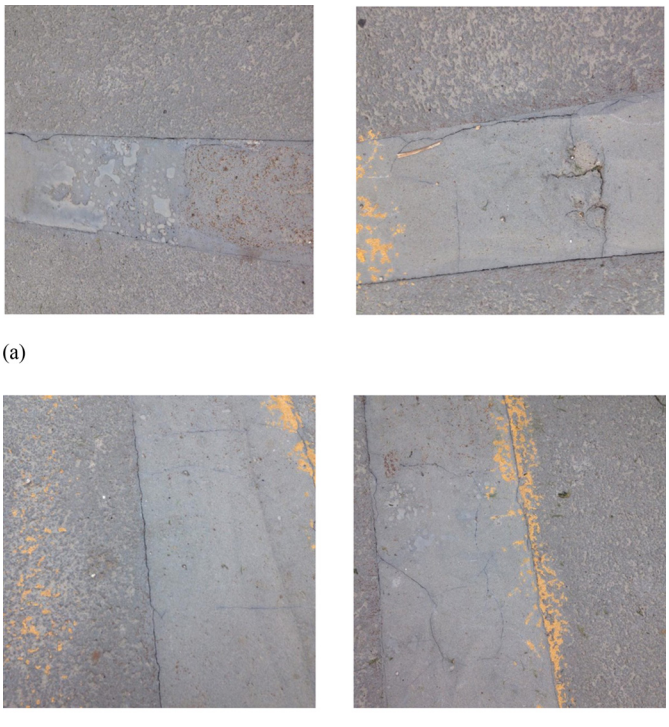

Fig. 1. Observed cracking in UHPC waffle deck bridge: (a) transverse joint; and (b) longitudinal joint.

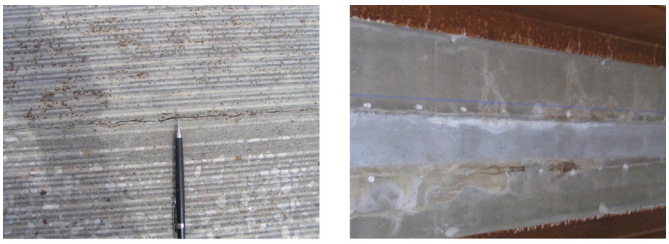

Fig. 2. Observed cracking in Keg Creek Bridge: (a) longitudinal joint; and (b) leakage due to interface cracking.

Objectives

The literature documents either bilinear AASHTO LRFD temperature distributions or linear temperature distributions used in the FE model to investigate the temperature effects on the behavior of the adjacent box beam bridges. Furthermore, calibrated FE modeling has not yet been conducted to investigate the effects of temperature distributions on the thermally induced stress in the shear keys. The main objectives of this study were as follows:

1. investigate the temperature distributions through the depth of an adjacent box beam bridge using field data and compare the results with AASHTO LRFD bridge design specifications,

Downloaded from ascelibrary.org by Iowa State University on 01/28/19. Copyright ASCE. For personal use only; all rights reserved.

2. validate the FE model with the field data and use the FE model to determine the thermally induced stress in UHPC connections and at the interface under temperature distributions; and
3. determine the temperature distribution that produces the largest thermally induced stress in UHPC shear key connections.

Bridge Details, Instrumentation, and Data Collection

In this study, the thermal behavior was investigated for an adjacent box beam bridge with a simple span 18.5 m (61 ft) long and 8.5 m (28 ft) wide. The bridge was constructed on Sollars Road in Fayette County, Ohio and contained seven box beams connected together using partial-depth UHPC shear keys, as presented in Fig. 3(a). The reinforcement in the beams was extended into the joint to create a noncontact lap splice staggered at 102 mm (4 in.), as presented in Fig. 3(b). The bridge was instrumented in various locations to investigate its behavior under changes in the thermal climate, as presented in Figs. 3(a, c, and d). The first three box beams were instrumented with vibrating wire strain gauges embedded in the beams and on the dowel bars, as presented in Fig. 3(c). Five strain gauges (three at midspan and two at quarter-span) were used in each beam to monitor the strain in longitudinal and transverse directions. Dowel bars in each beam were instrumented using vibrating wire strain gauges, and the gauge was installed at a distance of 50.8 mm (2 in.) from the threaded end of the dowel bar. A total of six dowel bars were instrumented using the

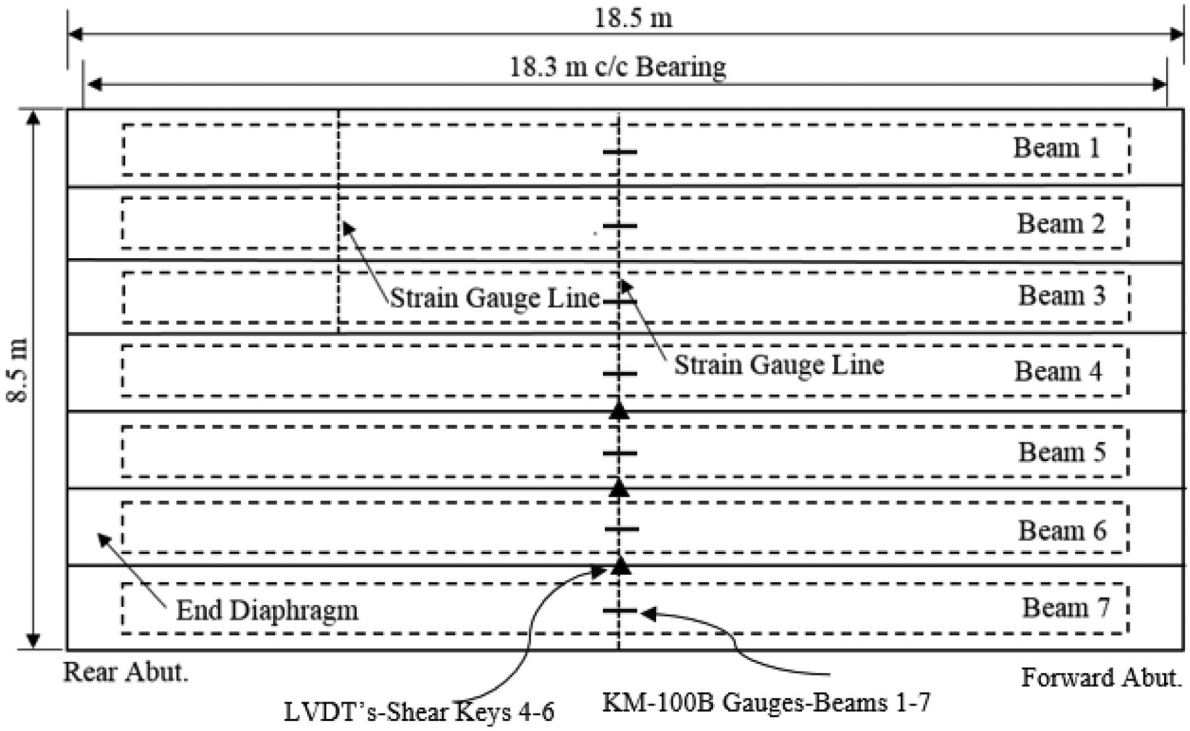

(a)

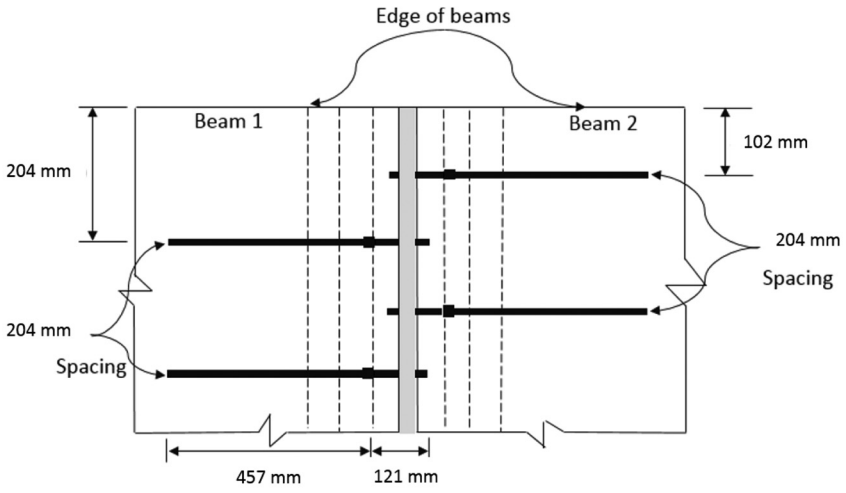

(b)

Fig. 3. Bridge description and instrumentation details: (a) exterior instrumentation details; (b) dowel bar details; (c) beams and dowel bar gauge details; and (d) shear key gauge details. c/c = center to center.

Downloaded from ascelibrary.org by Iowa State University on 01/28/19. Copyright ASCE. For personal use only; all rights reserved.

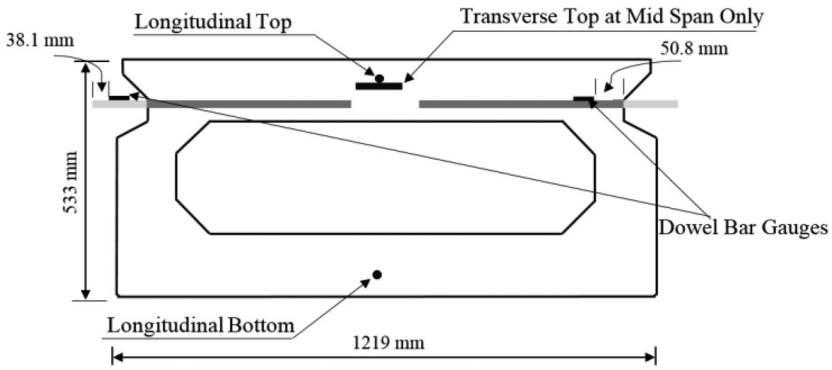

(c)

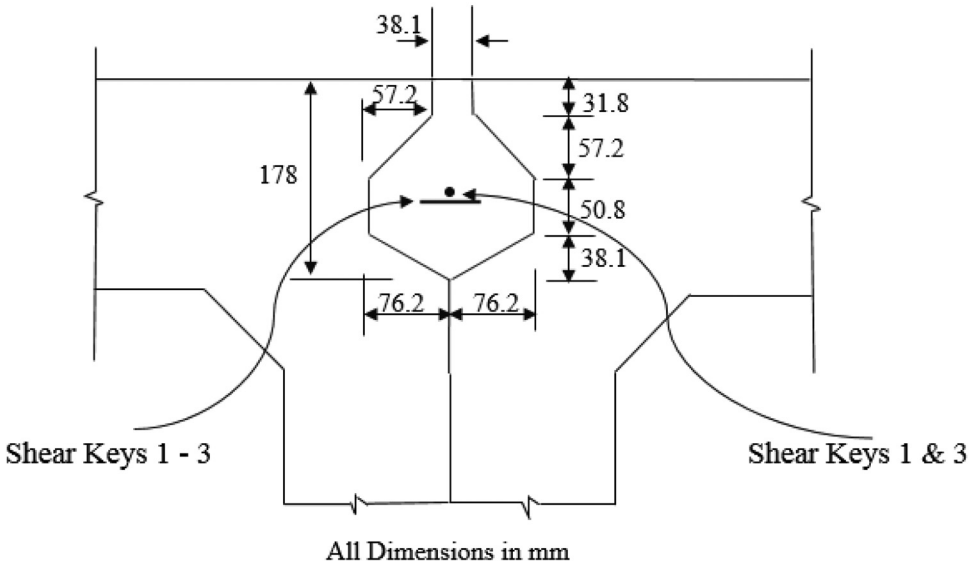

(d)

Fig. 3. (*Continued.*)

vibrating wire strain gauges. Beams 1, 2, and 3 each contained two instrumented dowel bars on the right side of the cross section, one at quarter-span and one at midspan. Six vibrating wire strain gauges were installed on six male threaded dowel bars. Each dowel bar was instrumented with one gauge at a distance of 38.1 mm (1.5 in.) from the threaded end. Two instrumented dowel bars were installed to the left side of Beams 2, 3, and 4, one at quarter-span and one at midspan. The three shear keys between Beams 1–4 were instrumented with vibrating wire strain gauges. Six short-length vibrating wire strain gauges were set in a transverse direction of all three shear keys, one at quarter-span and one at midspan. Shear keys 1 and 3 were also instrumented with one longitudinal gauge at quarter-span and one longitudinal gauge at midspan, as presented in Fig. 3(d). Seven KM Strain Transducer in the longitudinal direction were installed in gauge brackets that had been epoxied to the bottom of all beams. Joints 4, 5, and 6 were instrumented with three LVDTs at midspan. Two brackets were used to install the LVDTs transversely across the joint. The shear key joints were cast using UHPC containing 2% volume fraction of steel fibers. Ductal JS1000 UHPC, manufactured by Lafarge North America (Chicago, Illinois), was used to fill the shear keys. The proportions of the UHPC mix are displayed in Table 1. The joints were covered with plywood for curing purposes. The plywood forms were removed from the joints after 5 days. The UHPC reached a compressive strength of 151.7 MPa (22 ksi) after 28 days. More details about the description, fabrication, instrumentation, and testing can be found in the works by Steinberg et al. (2015) and Semendary et al. (2017a, b).

Table 1. Mix proportions for UHPC

Constituents	Amount (kg/m^3)
Premix	2,195
Water	130
Superplastizer (Chryso Premia 150, Chryso SAS, France)	30
Steel fiber	156

The temperature was recorded using thermocouples that were installed at multiple locations along the depth and length of the bridge. Beam 3 was instrumented with four thermocouples over the depth of the cross section, as presented in Figs. 4(a and b). These locations were chosen as an attempt to capture temperature distributions of the bridge and to compare with AASHTO (2016) for the state of Ohio. Fig. 4(b) presents the AASHTO LRFD-specified temperature gradient for the bridge. The temperature was also measured using the thermistor of the gauges that were embedded in beams/shear keys at both mid- and quarter-spans. In addition, temperature was recorded using external thermocouples attached to the bottom of the beams at midspan.

Downloaded from ascelibrary.org by Iowa State University on 01/28/19. Copyright ASCE. For personal use only; all rights reserved.

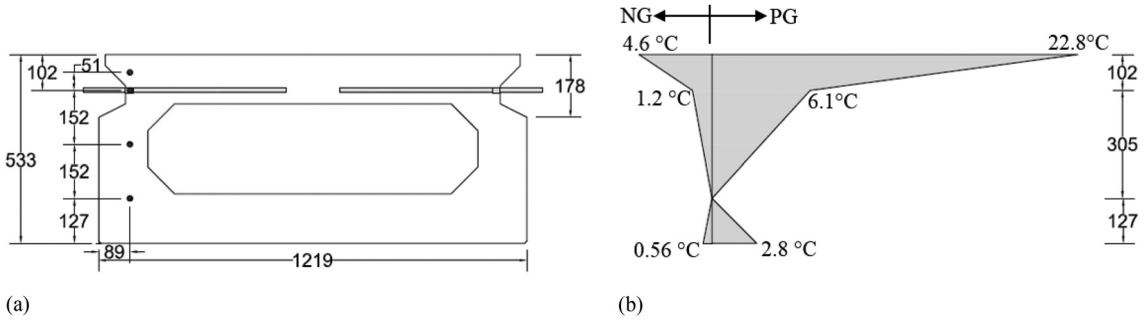

Fig. 4. Bridge instrumentation and temperature distribution: (a) thermocouple distribution over the height of Beam 3; and (b) positive gradients (PG) and negative gradients (NG) over the height (all dimensions in mm).

Downloaded from ascelibrary.org by Iowa State University on 01/28/19. Copyright ASCE. For personal use only; all rights reserved.

Data were collected from instrumentation during the period of August 8–16, 2014, after the bridge had been opened to traffic. During this period, the temperature was collected using thermocouples embedded in Beam 3 at midspan. In addition, the exterior temperature was recorded utilizing an external thermocouple attached to the bottom of Beam 4 at midspan. This period was used to investigate the behavior of the bridge due to hot weather. Data were also collected in December 2014 and January 2015 to monitor the behavior of the bridge when the temperature decreased during the winter months. However, the data from January 7 to 10, 2015 were chosen because this was the coldest period during the winter monitoring. During this period, the temperature was collected using thermocouples embedded in Beam 3 at midspan. In addition, the temperature was also recorded using external thermocouples attached to the bottom of Beams 1, 4, and 7 at midspan. The temperature was also monitored from July 9 to 14, 2015, 1 year after the construction of the bridge. During this period, the temperature was collected using thermocouples embedded in Beam 3 at midspan. In addition, the temperature was recorded using external thermocouples attached to Beams 1–7 at midspan.

Field Results

Maximum Positive and Negative Gradient Determination

The maximum temperature gradient can be defined as the largest positive and negative recorded differential temperature over the height of the superstructure (Rodriguez et al. 2014). The data from all periods revealed that the temperature of the thermocouple located at a height of 127 mm (5 in.) from the bottom changed slightly with time compared with other locations. Therefore, the temperature from this thermocouple was used as the baseline to determine the top and bottom temperature gradient for each period. This philosophy was also used by Rodriguez et al. (2014) to determine the temperature gradient. The maximum positive temperature gradients in the top flange were observed on August 15, 2014 at 1800; January 9, 2015 at 1630; and July 11, 2015 at 1800. Therefore, the temperature gradients from these measured periods were used to determine the temperature gradient over the height and compared with the temperature gradient from AASHTO (2016), as presented in Fig. 5(a). For the temperature gradient measured on August 15, 2014 at 1800, there was some consistency between AASHTO (2016) and the measured temperature gradient. The shape of the temperature gradient compared well with the AASHTO (2016) gradient. The maximum temperature gradient recorded along the depth during this time period was 13°C, which was the same as the AASHTO (2016) gradient for the specific depth. For the temperature gradient measured on January 9, 2015 at 1630, the measured temperature gradient was small compared with AASHTO (2016) and was approximately linear. The maximum temperature gradient recorded during this time period was 3°C, which was much less than 13°C from the AASHTO (2016) gradient at the specific depth. For the temperature gradient measured on July 11, 2015 at 1800, there was a consistency between the measured temperature gradient and AASHTO (2016). The shape of the temperature gradient compared well with the AASHTO (2016) gradient. The maximum temperature gradient recorded during this time period was 9°C, which was slightly less than 13°C from the AASHTO (2016) gradient at the specific depth.

The maximum negative temperature gradients in the top flange were observed on August 16, 2014 at 0830; January 8, 2015 at 0930; and July 11, 2015 at 0800. All measured temperatures for the periods were compared with AASHTO (2016), as presented in Fig. 5(b). For the temperature gradient measured on August 16, 2014 at 0830, there was some consistency between the measured temperature gradient and AASHTO (2016), except for the temperature gradient recorded at the bottom. The shape of the temperature gradient was a close match with the AASHTO (2016) gradient. The maximum temperature gradient recorded during this period was −1.5°C. The recorded temperature gradient was less than the negative temperature gradient from AASHTO (2016) at the specific depth. The bottom temperature gradient was –7°C, which was very high compared with AASHTO (2016). The same observation was noticed by Rodriguez et al. (2014). For the temperatures gradient measured on January 8, 2015 at 0930, there was consistency between the measured temperature gradient, especially for the bottom temperature gradient and the AASHTO (2016) temperature gradient. The maximum temperature gradient recorded during this period was –2°C. The temperature was slightly less than the negative temperature gradient from AASHTO (2016) at the specific depth. The bottom temperature gradient was –0.55°C, which was the same as AASHTO (2016). For the temperature gradient measured on July 11, 2015 at 0800, there was a difference between the measured temperature gradient and the AASHTO (2016) temperature gradient, especially for the top temperature. The maximum temperature gradient recorded during this period was –0.28°C, which was much less than the negative temperature gradient from AASHTO (2016) at the specific depth. The recorded bottom temperature gradient was –3°C, which was high compared with AASHTO (2016).

Measured Average Temperature

The maximum and minimum average daily temperatures were calculated using the measured daily temperatures collected by

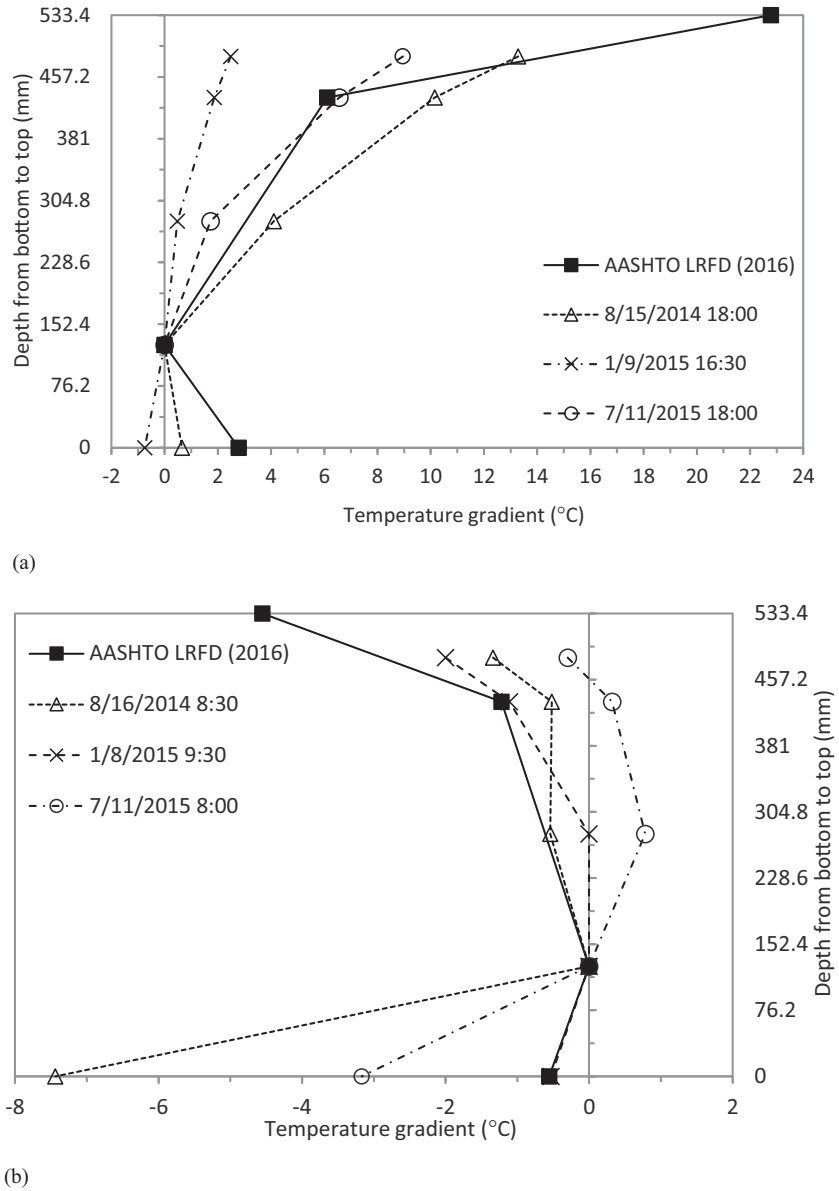

Fig. 5. Temperature gradient for Sollars Road Bridge compared with AASHTO (2016): (a) maximum positive; and (b) maximum negative.

thermocouples. The average temperature (T_{avg}) was calculated based on the temperature measured through the concrete cross section using Eq. (1) mentioned by Rodriguez et al. (2014)

$$T_{avg} = \frac{\sum A_i \times E_i \times \alpha_i \times T_i}{\sum A_i \times E_i \times \propto_i} \quad (1)$$

The cross section was divided into three horizontal segments, and the thermocouple was assumed approximately at the center of each segment. Constant temperature was assumed over the height of each segment. The modulus of elasticity was calculated by using the following equation from ACI 318-14 (ACI 2014):

$$E_c = 57000\sqrt{f'_c} \quad (2)$$

where f'_c = compressive strength of the concrete beam 3 months after casting, which was found to be 75.84 MPa (11 ksi). The calculated modulus of elasticity was found to be 41,286 MPa (5,985 ksi). The coefficient of thermal expansion of the concrete (α) was assumed to be a typical value of 10.8 μ/°C based on AASHTO (2016) for normal-weight concrete. The average temperature was calculated from the thermocouple data and is presented in Fig. 6. The average bridge temperature was within the range of Ohio maximum and minimum temperatures calculated according to AASHTO (2016). The recommended temperature range was found to be 43°C (110°F) to –23°C (–10°F). However, the maximum and minimum bridge temperature range determined from Eq. (1) was between 31°C (88°F) and –16°C (3°F). The results indicated that the AASHTO LRFD range was conservative in the design of box beam bridges with and without UHPC shear key connections.

Behavior of Bridge in Cold Weather

The maximum longitudinal and transverse tensile strains in the UHPC were observed during the monitoring period of January 7–10, 2015. The investigation was initiated on January 7, 2015 at 1400, where the reading from this time period was considered as the

Downloaded from ascelibrary.org by Iowa State University on 01/28/19. Copyright ASCE. For personal use only; all rights reserved.

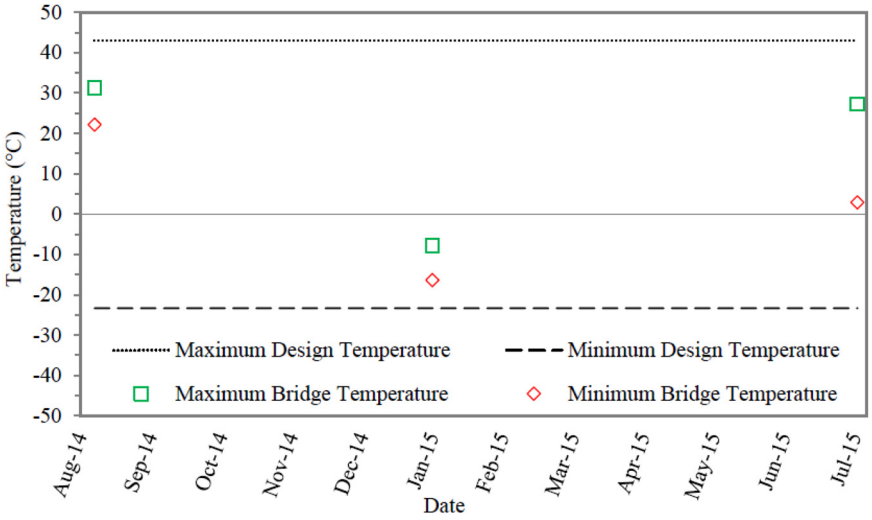

Fig. 6. Mean temperature for Sollars Road Bridge for the data collected during different periods compared with AASHTO (2016).

initial reading. The temperature distributions, temperature changes (calculated by subtracting the initial reading from the measured temperature of each specific time), and temperature gradient, which was investigated using the same concept previously discussed, are presented in Figs. 7(a–c). The bridge was under negative temperature during this measured period [Fig. 7(a)]. However, 12 temperature distributions were recognized based on 12 specific periods, which were initiated on January 7, 2015 at 1500 (only 1 h after the initial reading) and continued for every 3 h until January 9, 2015 at 0000. Fig. 7(a) demonstrates that the initial temperature, temperature after 1 hour, and temperature after 4 h were approximately linear. After the first 4 h, the temperature distribution changed to nonlinear and exhibited same trends until January 8, 2015 at 0900. Then, the nonlinear temperature distribution reversed for the remaining readings. Fig. 7(b) presents the changes in temperature with respect to the initial temperature. Fig. 7(c) presents the temperature gradients, which were approximately linear during the first 4 h. Then, negative temperature gradient was observed (where the temperatures in the top and bottom flanges were lower than the temperature in the web) from January 8, 2015 at 0300 until January 8, 2015 at 0900. This temperature distribution was anticipated to create tensile strain at both the top and bottom flanges and compressive strain at the web over the height of the beam. Positive temperature gradient was observed (where the temperatures in the top and bottom flanges were higher than the temperature in the web) from January 8, 2015 at 1500 until January 8, 2015 at 2100. This temperature distribution was anticipated to cause compressive strain in the top and bottom flanges and tensile strain in the web. However, two additional temperature gradients were recognized as follows: (1) the top flange and web temperature gradients were higher than the temperature gradient in the bottom flange (January 7, 2015 at 2100 and January 8, 2015 at 0000); and (2) the top flange and web temperature gradients were lower than the temperature gradient in the bottom flange (January 8, 2015 at 1200 and January 9, 2015 at 0000). These temperature gradients have not been considered in the current *LRFD Bridge Design Specifications* (AASHTO 2016). Furthermore, the type of longitudinal thermal strains (tension or compression) that these temperature gradients produce are unknown and require further investigation.

The change in longitudinal strains, transverse strains, and the joint opening/closing at midspan are presented in Tables 2–4, respectively. The results were divided into three categories based on the temperature gradient: (1) readings on January 7, 2015 at 1500 and 1800 (this reading was under approximately linear temperature gradient); (2) readings from January 7, 2015 at 2100 until January 8, 2015 at 0900, which were under either negative temperature gradient or a new temperature gradient (the top flange and web temperature gradient were higher than the temperature gradient in the bottom flange); and (3) readings from January 8, 2015 at 1200 until January 9, 2015 at 0000, which were under either positive temperature gradient or new temperature gradient (the top flange and web temperature gradients were lower than the temperature gradient in the bottom flange). The readings on January 8, 2015 at 1200 represented a change from negative to positive temperature gradient.

Tensile strain was observed in Beams 1–7 at the exterior bottom surface under Categories 1 and 2 and compressive strain was observed under Category 3 (Table 2). The interior top flange strains in Beams 1–3 were opposite to the strains of the exterior bottom flange. This indicates that the bridge did not exhibit uniform strain distribution. The longitudinal strain and temperature distributions along the depth of Beams 1–3 for data collected on January 7, 2015 at 2100; January 8, 2015 at 0600; January 8, 2015 at 1200; and January 8, 2015 at 1800 are presented in Figs. 8(a–d) and Figs. 9(a–d), respectively. The temperature distributions on January 7, 2015 at 2100 and January 8, 2015 at 1200 represent temperature gradient, which does not exist in the AASHTO *LRFD Bridge Design Specifications* (AASHTO 2016), whereas the temperature distributions on January 8, 2015 at 0600 and January 8, 2015 at 1800 represent negative and positive temperature gradients, respectively. For the temperature distribution on January 8, 2015 at 0600, the temperature gradients in the top and bottom were lower than the temperature gradient in the web, which is consistent with the AASHTO (2016) negative temperature gradient. For the temperature distribution on January 8, 2015 at 1800, the temperature gradients in the top and bottom were higher than the temperature gradient in the web, which is consistent with the AASHTO (2016) positive temperature gradient. The longitudinal strain distribution along the depth in Beams 1–3 was nonlinear and was inverse to the temperature, as presented in Figs. 8(a–d). This indicates the longitudinal strain distributions for the temperature gradient presented in Figs. 9(a and c) were also inverse to the trend of the temperature. Furthermore, the highest tensile strain in the top flange was noticed under a new temperature gradient presented in Fig. 9(c).

Downloaded from ascelibrary.org by Iowa State University on 01/28/19. Copyright ASCE. For personal use only; all rights reserved.

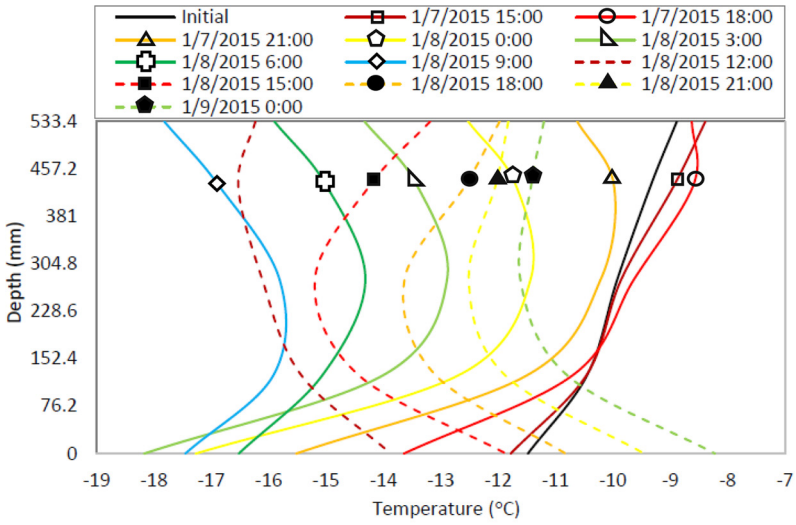

(a)

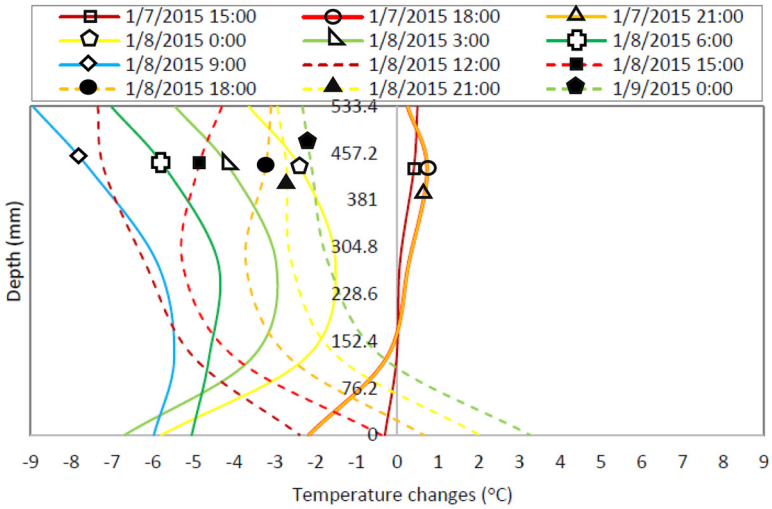

(b)

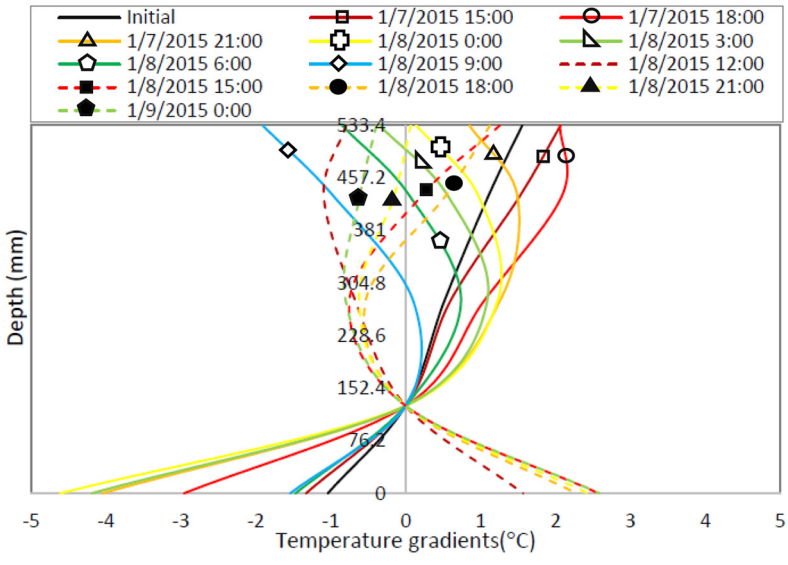

(c)

Fig. 7. Temperature distribution over the height of Beam 3: (a) total temperature; (b) temperature changes; and (c) temperature gradients (initial on July 7 at 1400).

Downloaded from ascelibrary.org by Iowa State University on 01/28/19. Copyright ASCE. For personal use only; all rights reserved.

Table 2. Longitudinal strain change in beams and shear keys

	Exterior beam bottom							Interior beam bottom			Interior beam top			UHPC shear key	
Date (time)	1	2	3	4	5	6	7	1	2	3	1	2	3	1	3
January 7 (0500)	—	—	—	—	—	—	—	—	—	—	—	−5	−5	—	−5
January 7 (1800)	15	10	10	10	15	10	15	—	—	5	−5	−15	−20	−5	−10
January 7 (2100)	20	15	10	15	15	15	20	—	—	—	−10	−20	−20	—	—
January 8 (0000)	30	20	15	20	20	20	25	10	5	5	−5	−15	−10	—	5
January 8 (0300)	30	20	15	20	20	20	25	10	10	5	−5	−15	−5	5	15
January 8 (0600)	25	10	10	15	15	15	25	15	15	10	5	−5	−5	15	25
January 8 (0900)	25	15	5	15	15	20	30	15	10	5	10	—	5	35	40
January 8 (0200)	—	−5	−10	−5	−5	—	5	10	5	5	25	25	20	50	50
January 8 (0500)	−5	−10	−10	−10	−10	−5	−5	10	5	5	15	10	5	45	30
January 8 (1800)	−5	−5	−10	−5	−5	−5	−5	10	5	5	5	—	−5	35	25
January 8 (0100)	−10	−5	−10	−10	−5	−5	−5	10	—	—	5	—	−5	35	30
January 9 (0000)	−10	−5	−15	−10	−10	−5	−5	10	—	—	15	10	—	30	30

Note: —, reading less than ±2 microstrain.

Table 3. Transverse strain change in beams, shear keys, and dowel bars

	Interior beam top			UHPC shear key			Dowel beam			Dowel shear key		
Date (time)	1	2	3	1	2	3	1	2	3	1	2	3
January 7 (1500)	—	−5	−5	—	—	—	—	—	−5	—	—	—
January 7 (1800)	−5	−10	−15	—	−10	−5	−5	−5	−10	−5	−5	−5
January 7 (2100)	−5	−15	−20	—	−10	−5	—	−5	−5	−5	−10	−10
January 8 (0000)	—	−10	−20	5	−5	—	5	−5	5	−5	−10	−10
January 8 (0300)	5	−10	−10	5	—	5	15	5	10	−5	−10	−10
January 8 (0600)	15	—	−5	10	5	10	20	10	20	−5	−10	−10
January 8 (0900)	25	10	5	15	15	15	30	20	30	—	−5	−10
January 8 (1200)	30	30	30	15	30	20	30	35	40	5	10	5
January 8 (1500)	30	20	30	10	25	10	20	40	25	5	10	—
January 8 (1800)	25	15	15	10	10	5	15	30	15	5	5	—
January 8 (2100)	20	15	15	5	10	5	15	25	15	5	5	—
January 9 (0000)	20	15	15	5	10	5	15	25	15	5	5	—

Note: —, reading less than ±2 microstrain.

Table 4. Joint movement (mm)

	Joint	
Date (time)	4	5
January 7 (1500)	−0.01	−0.01
January 7 (1800)	−0.06	−0.04
January 7 (2100)	−0.06	−0.04
January 8 (0000)	−0.06	−0.04
January 8 (0300)	−0.05	−0.03
January 8 (0600)	−0.03	−0.02
January 8 (0900)	−0.02	−0.01
January 8 (1200)	0.04	0.03
January 8 (1500)	0.01	0.01
January 8 (1800)	−0.01	0.00
January 8 (2100)	0.01	0.01
January 9 (0000)	0.02	0.02

The longitudinal strain in the shear key was in compression under Category 1, and then only tensile strain was observed under Categories 2 and 3. This indicates that the nonlinear temperature gradient has more effect on the longitudinal behavior of UHPC connections by creating tensile strain with respect to the types of gradient. In addition, the longitudinal tensile strain in the UHPC was higher than the value in the beams. This behavior might be related to the difference in the coefficient of thermal expansion, which caused the UHPC to expand or contract more than the concrete beam. This difference could create longitudinal shear stress, which may cause longitudinal cracks at the interface. For instance, Shear key 1 was located between Beams 1 and 2. The highest longitudinal tensile strain in Shear key 1 was 50 $\mu\varepsilon$ on January 8, 2015 at 1200. The longitudinal tensile strain in the top flanges of both Beams 1 and 2 was 25 $\mu\varepsilon$ at that time. The longitudinal strain was measured at midwidth of the beams. However, the longitudinal strain in the shear key was measured at the center of the key. If a linear strain distribution in the transverse direction was assumed across the width between the center of the beam and the center of the shear key, the strain at the interface would be 45 $\mu\varepsilon$. This assumption was based on the approximate linear behavior between the centers of the beams and joints from the plot of the transverse strain across the width of the bridge, as presented in Fig. 10. The modulus of elasticity of the concrete beam was determined from Eq. (2), and the modulus of elasticity of the UHPC was calculated using the following equation from Russell and Graybeal (2013):

$$E_c = 49{,}000\sqrt{f_c'} \tag{3}$$

where f_c' = compressive strength of the UHPC after 28 days, which was found to be 151.7 MPa (22 ksi). The modulus of elasticity of the UHPC was found to be 50,111 MPa (7,268 ksi). The longitudinal strains caused longitudinal stresses of 1.86 MPa (0.27 ksi) in the concrete beam and 2.3 MPa (0.33 ksi) in the UHPC. Therefore, the difference between the longitudinal stresses in the UHPC and concrete beam caused a longitudinal shear stress of 0.44 MPa (0.1 ksi) in the longitudinal direction. The maximum longitudinal shear stress occurred when the top flange and web temperature gradients were lower than the temperature gradient in the bottom flange. The period of time represented a change from negative to positive temperature gradient [Fig. 7(c)]. The interface shear strength should be higher than 0.44 MPa (0.1 ksi) to prevent the longitudinal cracks at the interface. However, the interface shear strength depends on the surface preparation, moisture content, and the normal compressive force across the interface. A push-off test was conducted by the authors to explore the interface bond strength under shear between

Downloaded from ascelibrary.org by Iowa State University on 01/28/19. Copyright ASCE. For personal use only; all rights reserved.

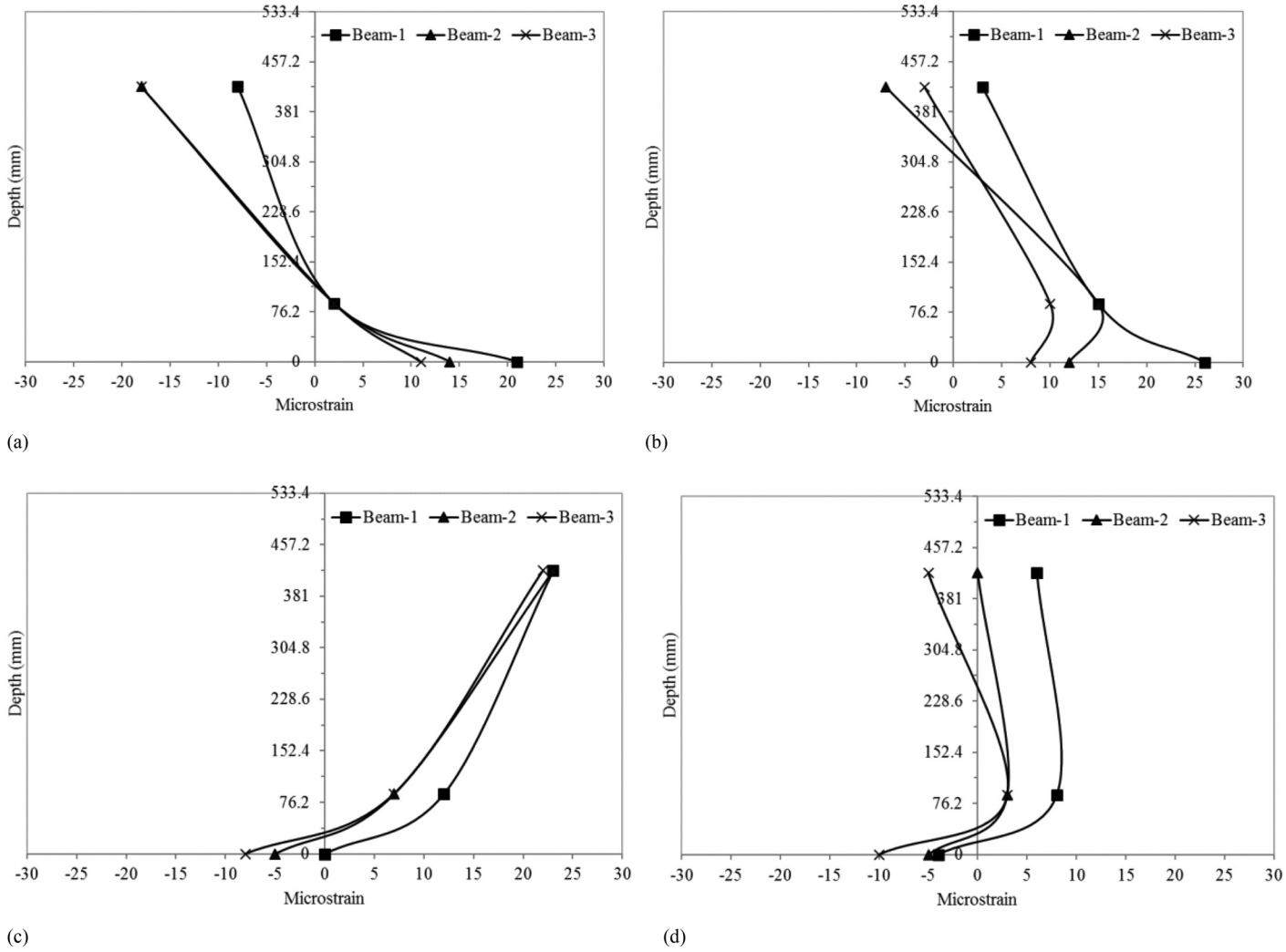

Fig. 8. Strain distribution over depth in Beams 1–3 for different time periods: (a) January 7, 2015 at 2100; (b) January 8, 2015 at 0600; (c) January 8, 2015 at 1200; and (d) January 8, 2015 at 1800.

high strength concrete and UHPC using an exposed aggregate surface condition. A brief description of the experimental program will be presented in the "FE Model" section. The interface shear strength was found to be 4.91 MPa (0.71 ksi). Therefore, the calculated shear stress at the interface was not high enough to cause interfacial cracking, and the interface bond strength was high enough to resist the shear stress from temperature changes. The maximum change in longitudinal tensile strain of 50 $\mu\varepsilon$ in UHPC was observed on January 8, 2015 at 1200. This strain was equivalent to a tensile stress of 2.5 MPa (0.36 ksi) by considering the modulus of elasticity of UHPC. The allowable tensile strength of UHPC must be greater than this value to prevent the transverse cracks in UHPC connections. The maximum allowable tensile strength of UHPC used in this study was 6.83 MPa (0.99 ksi), and therefore, no cracks in the UHPC were anticipated based on the temperature level that was considered.

The transverse behavior in the top flanges of Beams 1–3 was approximately the same as the longitudinal behavior in the top flanges as presented in Table 3. The maximum transverse strain occurred at the same time period (January 8, 2015 at 1200). This means that both directions exhibited the same deformation on the top of the bridge. This behavior does not occur under mechanical load because Poisson's effects would cause an opposite deformation in the transverse direction compared with the longitudinal direction. The UHPC transverse shear key behavior was also consistent with the longitudinal behavior of shear keys. However, the UHPC in the longitudinal direction typically exhibited higher tensile strain than the strain in the transverse direction. Although the coefficient of thermal expansions was different, the transverse behavior of the shear keys was also consistent with the transverse behavior in the beams. The transverse strain and temperature distributions along the half width of the bridge are presented in Figs. 10(a and b). The transverse strain distribution was also generally nonlinear as observed for the longitudinal strain distribution along the depth. However, the transverse strain distribution between the center of the beam and the center of the shear key was approximately linear. The transverse strain changed from negative on January 7, 2015 at 2100 to positive on January 8, 2015 at 1200 when the temperature decreased by approximately 7°C. Therefore, more decrease in temperature was anticipated to create higher tensile strain in the shear keys. The maximum transverse tensile strain was observed when the temperature in the shear keys was slightly less than the temperature in the beams. The transverse behavior may also be affected by the longitudinal behavior and the temperature gradient along the depth. The decrease in temperature in the exterior beam was higher than

Downloaded from ascelibrary.org by Iowa State University on 01/28/19. Copyright ASCE. For personal use only; all rights reserved.

Downloaded from ascelibrary.org by Iowa State University on 01/28/19. Copyright ASCE. For personal use only; all rights reserved.

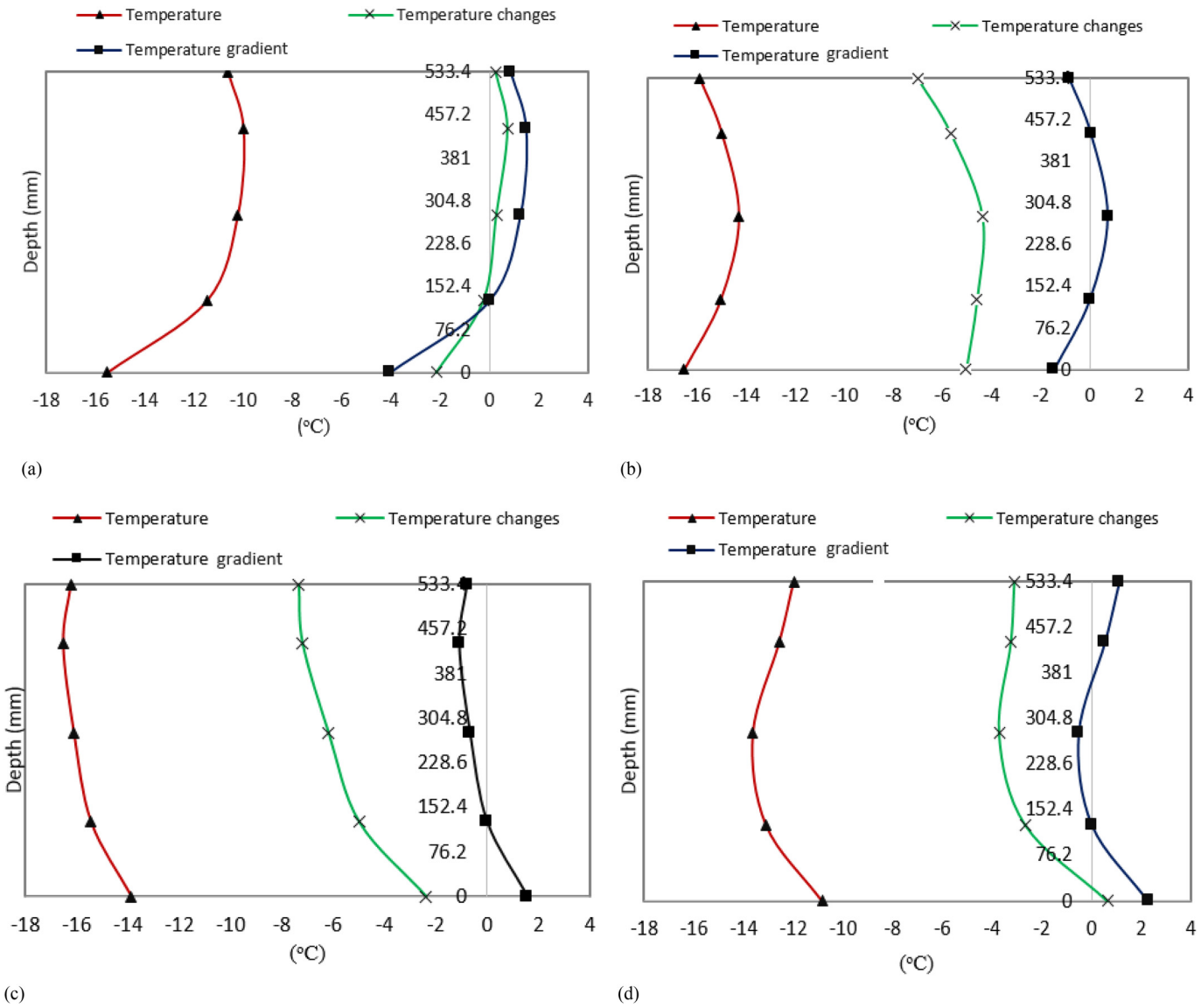

Fig. 9. Temperature, temperature changes, and temperature gradients over height for different time periods: (a) January 7, 2015 at 2100; (b) January 8, 2015 at 0600; (c) January 8, 2015 at 1200; and (d) January 8, 2015 at 1800.

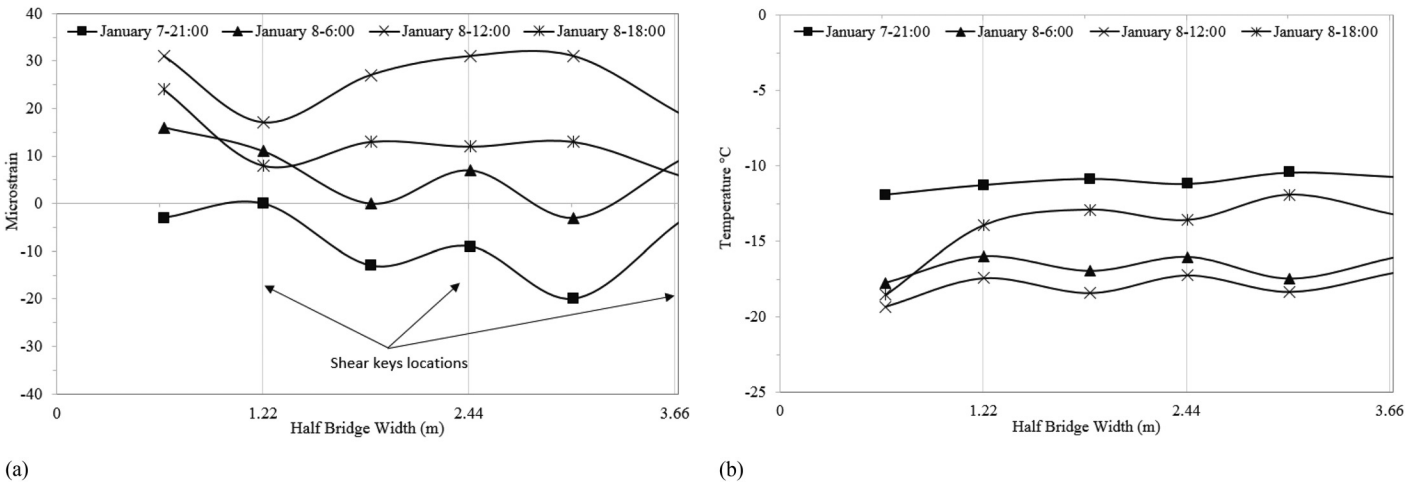

Fig. 10. Strain distribution and temperature distributions along the width of the bridge: (a) strain; and (b) temperature.

the interior beams, which indicates there was a slight temperature gradient in the transverse direction.

The behavior of the dowel bars for the portion embedded in Beams 1–3, corresponding to the temperature, also followed the same trend as the behavior of Beams 1–3 in the transverse direction. The tensile/compressive strain in the dowel bars was approximately the same as in the beam. However, the dowel bars embedded in Shear keys 1–3 typically exhibited less strain and sometimes an opposite strain compared to the portion embedded in Beams 1–3. For concrete, the coefficient of thermal expansion was taken as 10.8 μ/°C based on AASHTO (2016) for normal-weight concrete. For UHPC, the coefficient of thermal expansion was taken as 15.3 μ/°C based on the recommendation by Russell and Graybeal (2013). For the dowel bars, the coefficient of thermal expansion was taken as 11.7 μ/°C based on AASHTO (2016). The coefficient of thermal expansion of steel was slightly higher than that of concrete but was much less than that of UHPC. Therefore, this could be a reason for the low strain in the portion of the dowels embedded in the keys compared with the portion embedded in the beams. The strain of the dowel bars embedded in the shear keys was also generally less than the transverse strain in the UHPC. This could also be related to the difference in the coefficient of thermal expansion between the UHPC and steel. The maximum observed tensile strain from almost all instrumentation in the transverse direction occurred at 1200 on January 8, 2015. During this time period, the top flange and web were under a negative temperature gradient and the bottom flange was under a positive temperature gradient (the temperature gradient changed from negative to positive). Under a negative temperature gradient in the top flange, the beams and shear keys tried to contract individually. However, the interface bond strength tried to resist this movement, which created tensile strain. Therefore, the interface bond strength should be higher than the observed tensile stress in beams or shear keys to prevent interface failure. The maximum transverse tensile strain in Beams 1–3 was approximately 30 $\mu\varepsilon$. This strain was equivalent to a tensile stress of 1.31 MPa (0.19 ksi) by considering the modulus of elasticity of concrete. This tensile stress was lower than the tensile strength of the concrete, which was 5.24 MPa (0.787 ksi), and therefore, cracks were not anticipated to occur in the beams. The maximum tensile strain in UHPC was also 30 $\mu\varepsilon$, which was equivalent to a tensile stress of 1.55 MPa (0.225 ksi) by considering the modulus of elasticity of UHPC. This value was lower than the tensile strength of UHPC, which was 6.83 MPa (0.99 ksi). The interface bond strength should be greater than 1.55 MPa (0.225 ksi) to prevent interface debonding. The interface bond strength under a tensile stress state was also investigated by the authors. The experimental test is discussed later in the "FE Model" section. The minimum interface bond strength between cast-in-place UHPC and precast high-strength concrete after 28 days for exposed aggregate surface preparation was found to be 1.76 MPa (0.254 ksi). The transverse tensile stress was slightly less than the interface bond strength. The interface bond strength of UHPC with concrete was investigated using a flexural beam test for different surface preparations (Graybeal et al. 2017). The interface bond strengths were approximately 0.413 MPa (0.06 ksi) and 1.38 MPa (0.2 ksi) for pressure wash and sandblast surfaces, respectively. However, the interface bond strength was 4.27 MPa (0.62 ksi) for an exposed aggregate surface. Phares et al. (2013) reported that the interface bond strength using direct tension and flexural beam tests at 4 days varied between 0.63 and 3.5 MPa (0.091 and 0.51 ksi). The interface bond strength highly depends on the surface preparation and testing methods. Therefore, the observed tensile stress across the interface could cause interface failure in the case of weak bonding for the temperature level that was observed.

The movements of Joint 4 (between Beams 4 and 5) and Joint 5 (between Beams 5 and 6) are presented in Table 4. A positive joint movement means the joint was closing, and a negative value means the joint was opening. The movement of the joint occurred due to temperature changes. The maximum joint closing was observed on January 8, 2015 at 1200. The maximum transverse tensile strains in beams, shear keys, and dowel bars were also observed during this time period. This could be one reason for the transverse tensile strain at the top because the joint was closing at the bottom.

FE Model

The FE model for the Sollars Road Bridge was developed using Abaqus version 6.14 software to investigate the behavior of the bridge due to both truck and temperature loads. The model was calibrated and validated under static truck-load testing and was able to capture the behavior of the bridge (Semendary et al. 2017b). However, the model in this study was used to investigate the behavior of the bridge under different temperature distributions, and therefore, more validation was needed. The model was constructed from different parts, which included seven box beams, six shear keys, prestressed strand, longitudinal reinforcement, dowel bars, and diaphragms. Three-dimensional linear elastic brick elements (C3D8R) were used to model every part. The modulus of elasticity of the concrete beam was calculated by using Eq. (2), and Poisson's ratio was taken as 0.2. The modulus of elasticity of UHPC was calculated using Eq. (3) and was found to be 50,111 MPa (7,268 ksi), and Poisson's ratio was taken as 0.18. The prestressed strand was also modeled by assuming an elastic modulus of 196,500 MPa (28,500 ksi) and Poisson's ratio of 0.3. The longitudinal reinforcement and the dowel bars were modeled by assuming an elastic modulus of 200,000 MPa (29,000 ksi) and Poisson's ratio of 0.3. For concrete, the coefficient of thermal expansion was taken as 10.8 μ/°C based on AASHTO (2016) for normal-weight concrete. For UHPC, the coefficient of thermal expansion was taken as 15.3 μ/°C based on the recommendation by Russell and Graybeal (2013). For the longitudinal reinforcement, prestressed strands, and dowel bars, the coefficient of thermal expansion was taken as 11.7 μ/°C based on AASHTO (2016).

The partition option in Abaqus was implemented at different locations to simplify the geometry, which assisted in obtaining a more-uniform mesh size. Each part was meshed individually with the box beams, shear keys, longitudinal reinforcement, prestressed strand, and end diaphragms seeded to 76 mm (3 in.) along the longitudinal direction. The cross section of each part was meshed individually to obtain a more-uniform size. Also, a finer mesh was used in the location of the shear keys. A tie constraint using the surface-to-surface option in Abaqus was used to model the interaction between the end diaphragms and box beam because both components were cast together. An embedded constraint was used to model the interaction between the concrete or UHPC and the longitudinal reinforcement, prestressed strand, and dowel bars. The most important interaction in the model was the interface between the UHPC and the box beams because the debonding failure could be investigated by using the most-accurate representation of the interface. The interaction between the UHPC and precast concrete was modeled using a combination of surface-based cohesive behavior combined with compressive and friction behavior. The surface-based cohesive behavior (traction-separation behavior) allows for the debonding failure mode. The traction-separation model consisted of initially linear elastic behavior followed by the initial and evolution of damage. The model used the initial normal (σ_n^o) and shear stresses (τ_s^o, τ_t^o) at the interface, along with those calculated

Downloaded from ascelibrary.org by Iowa State University on 01/28/19. Copyright ASCE. For personal use only; all rights reserved.

under load $(\sigma_n,\ \tau_s,\ \tau_t)$. The model assumed a linear elastic traction separation prior to damage. The damage initiates when a quadratic interaction function of the contact stress ratios is equal to 1, as demonstrated by Eq. (4)

$$\left\{\frac{\langle t_n\rangle}{t_n^o}\right\}^2+\left\{\frac{t_s}{t_s^o}\right\}^2+\left\{\frac{t_t}{t_t^o}\right\}^2=1 \tag{4}$$

The values used in the model were calculated based on the experimental test conducted by the authors. The interface bond strength between precast high-strength concrete (HSC) and cast-in-place UHPC under direct tension was measured using ASTM C1404/C1404M (ASTM 2003). The HSC reached a compressive strength of 56 MPa (8.1 ksi) and the UHPC reached a compressive strength of 113 MPa (16.5 ksi) after 28 days. The composite specimen of HSC–UHPC was 76 mm in diameter and 152 mm long. The composite specimen was tested under direct tension, and the bond-slip relationship is presented in Fig. 11(a). The solid line in Fig. 11(a) represents the measured bond-slip relationship, and the dashed line represents the proposed bond-slip relationship. The interface bond-strength parameters were driven by assuming a bilinear bond-slip relationship, and the values are presented in Table 5. The interface bond strength between HSC and cast-in-place UHPC under direct shear was also measured by the authors using a push-off test. The composite specimen was tested under direct shear and the bond-slip relationship is presented in Fig. 11(b). The solid line in Fig. 11(b) represents the measured bond-slip relationship, whereas the dashed line represents the proposed relationship. The interface bond-strength parameters were driven from the bond-slip relationship, and the values are presented in Table 5. In both test methods, the exposed aggregate at the interface was either broken or sheared off, which indicates that the measured bond strength represented the cohesion/adhesion at HPC–UHPC interfaces. The interface surface condition of the Sollars Road Bridge was consistent with the experimental test, which indicates the measured value could be used in in the modeling of beam–shear key interface. The boundary conditions were defined in the model. The pin roller, with a longitudinal spring of 2.6 kN/mm (15 kip/in.), was calibrated with static truck-load data and, therefore, utilized in this model.

FE Model Validation

The temperature load considered in the model validation was determined for the data collection period of January 7–10, 2015, because the highest transverse and longitudinal tensile strains in the shear

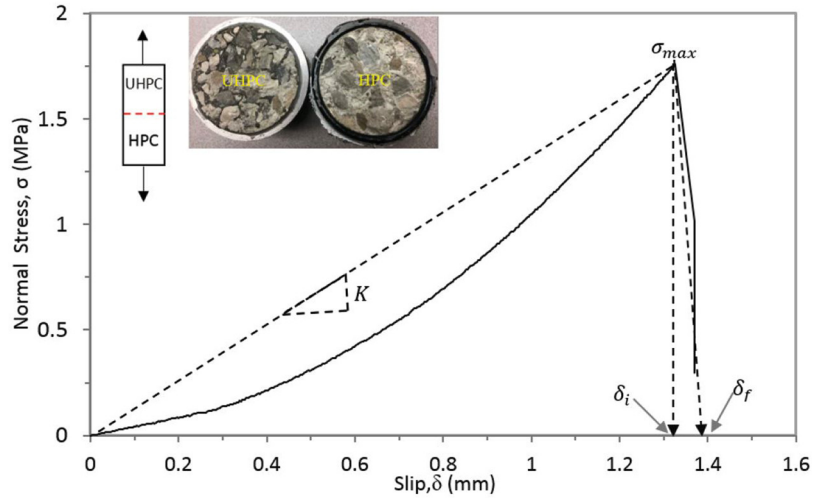

(a)

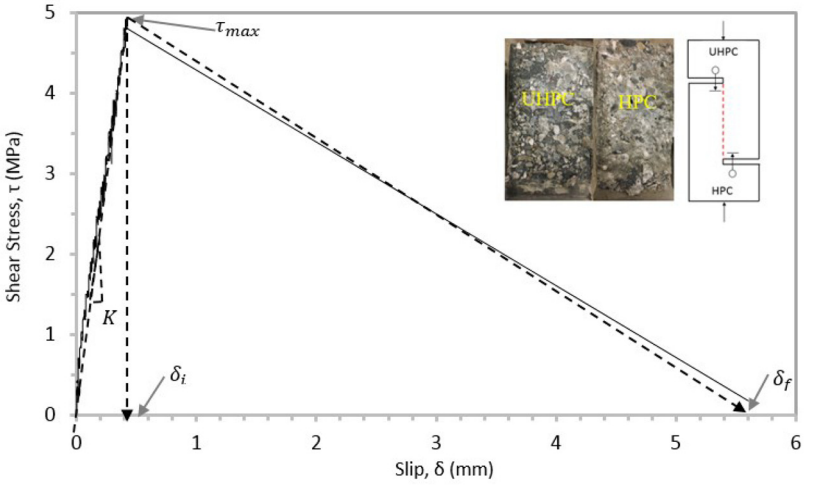

(b)

Fig. 11. Proposed bond versus slip model at HSC–UHPC interface for an exposed aggregate surface: (a) direct tension; and (b) direct shear.

J. Bridge Eng., 2019, 24(2): 04018115

Downloaded from ascelibrary.org by Iowa State University on 01/28/19. Copyright ASCE. For personal use only; all rights reserved.

Table 5. Estimated UHPC interface parameters

Parameter	Deformed
Traction separation low	
σ_n^o (MPa)	1.76
K_{nn} (N/mm^3)	1.325
G_{cr} (N/mm)	1.202
τ_s^o (MPa)	4.91
τ_t^o (MPa)	4.91
K_{ss} (N/mm^3)	12.1
K_{tt} (N/mm^3)	12.1
G_{cr} (N/mm)	13.76
Friction model	
μ	1

keys were observed during this period. The temperature on January 7, 2015 at 1400 was used in Abaqus as the initial temperature using a predefined field option. The temperatures from all thermocouples, which were distributed over the height of Beam 3, were used for each time period. This resulted in a nonlinear temperature distribution along the depth. A constant temperature was assumed along the length/width of the bridge. However, the bridge may also exhibit a temperature difference along its length and/or width, but this was not considered in the model. By defining the initial and final temperatures in Abaqus, the calculated strain corresponded to the effects of temperature changes only. The same concept was used in the validation of the model by Hedegaard et al. (2013). The temperature and strain were recorded at 15-min intervals when the data were collected in the field. However, only four time periods were considered in the FE model to reduce the cost of the analysis. Furthermore, each time period was chosen to represent different temperature distributions. The temperature distribution used in the FE model was taken from the data collected on January 7, 2015 at 2100; January 8, 2015 at 0600; January 8, 2015 at 1200; and January 8, 2015 at 1800, as presented in Fig. 9.

Results from the FE model and from the field were compared for each specific time period. Table 6 presents a comparison of the strain at the exterior bottom flange of Beams 1–7 in the longitudinal direction at midspan. The values compared well, especially for Beam 3, because the temperature used in the model was taken from the thermocouples embedded in Beam 3. Positive tensile strain was observed based on both the field data and the FE model in the exterior bottom of Beams 1 and 7 for the time periods January 7, 2015 at 2100 and January 8, 2015 at 0600. The bridge was subjected to either the negative temperature gradient during these periods because the temperatures in the top and bottom of the beam were lower than the temperature in the web, or the new temperature gradient (the top flange and web temperature gradients were higher than the temperature gradient in the bottom flange) [Fig. 7(c)]. For the time period of January 8, 2015 at 1200 and 1800, negative compressive strain was observed at the exterior bottom of Beams 1–7. The bridge was subjected to either positive temperature gradient because the top and bottom temperatures of the beam were higher than the temperature in the web, or the new temperature gradient (the top flange and web temperature gradients were lower than the temperature gradient in the bottom flange) as previously presented in Fig. 7(c).

The strains in Shear keys 1 and 3 in the longitudinal direction at mid- and quarter-spans were also compared with the results from the FE model, as presented in Table 7. Tensile strain was observed in the shear keys in the longitudinal direction except for the time period of January 7 at 2100. The strains from the model corresponded fairly well with the field data at both mid- and quarter-spans. The highest longitudinal tensile strain in the shear keys based on both field and modeling data was observed on January 8, 2015 at 1200. As mentioned earlier, this time period represents the transition from the negative to the positive temperature gradient.

Table 6. Exterior bottom flange strains in Beams 1–7

		Exterior bottom flange of beams						
Date (time)	Results	1	2	3	4	5	6	7
January 7 (2100)	Field	20	10	10	15	15	15	20
	FE model	15	15	15	20	15	15	15
January 8 (0600)	Field	30	10	10	15	15	15	25
	FE model	10	15	15	15	15	15	10
January 8 (1200)	Field	—	−5	−10	−5	−5	—	5
	FE model	−5	—	—	—	—	—	—
January 8 (1800)	Field	−5	−5	−10	−5	−5	−5	−5
	FE model	−15	−10	−10	−10	−10	−10	−15

Note: —, reading less than ±2 microstrain.

Table 7. Longitudinal strain in Shear keys 1 and 3 at mid- and quarter-spans

		Shear key 1 ($\mu\varepsilon$)		Shear key 3 ($\mu\varepsilon$)	
Date (time)	Result types	Midspan	Quarter-span	Midspan	Quarter-span
January 7 (2100)	Field	—	—	—	5
	FE model	—	—	—	—
January 8 (0600)	Field	15	25	30	30
	FE model	20	20	20	20
January 8 (1200)	Field	50	50	50	40
	FE model	30	30	35	35
January 8 (1800)	Field	35	40	25	15
	FE model	15	15	15	15

Note: —, reading less than ±2 microstrain.

Discussion: Behavior of UHPC Connection

Longitudinal cracks in shear keys develop whenever the transverse tensile stress in the shear keys is higher than the allowable tensile strength of the grout material or the stress at the interface is higher than the interface bond strength. These two types of failure were investigated in the FE model under different temperature distributions. The maximum tensile strains in shear keys and dowel bars were investigated based on the FE model, as presented in Table 8. The FE model also replicated the field results because the maximum transverse and longitudinal tensile strains were observed on January 8, 2015 at 1200 (transition from the negative to positive temperature gradient) as presented in Figs. 12(a and b). The maximum transverse tensile strain in the shear keys was observed near the support, as presented in Fig. 12(a). Furthermore, the transverse tensile strain was the main component in the maximum principal tensile strain for this time period. The maximum transverse/longitudinal tensile strain from the FE model was 40 $\mu\varepsilon$, whereas the maximum values from the field were 30 and 50 $\mu\varepsilon$, respectively. The maximum axial tensile strain in the dowel bars was also observed on January 8, 2015 at 1200 (transition from the negative to positive temperature gradient) near the support, which corresponded to the location of transverse tensile strain in the shear key, as presented in Fig. 12(c). This strain was equivalent to the axial stress of 148 MPa (21.5 ksi) by considering the modulus of elasticity of steel and was located at the end of the connection near the support. The maximum axial tensile strain in the dowels was observed at the beam–shear key interface near the support. However, the strain gauge on the dowel was

Downloaded from ascelibrary.org by Iowa State University on 01/28/19. Copyright ASCE. For personal use only; all rights reserved.

Table 8. Maximum strain in shear key and transverse reinforcement based on FE model

Date (time)	Strain in shear keys ($\mu\varepsilon$)			Strain in dowel bars ($\mu\varepsilon$)	
	Axial tensile strain	Longitudinal strain	Maximum principal tensile strain	Axial strain	Maximum principal tensile strain
January 7 (2100)	6	20	20	68	71
January 8 (0600)	32	39	54	582	600
January 8 (1200)	41	40	69	740	762
January 8 (1800)	20	23	32	360	365

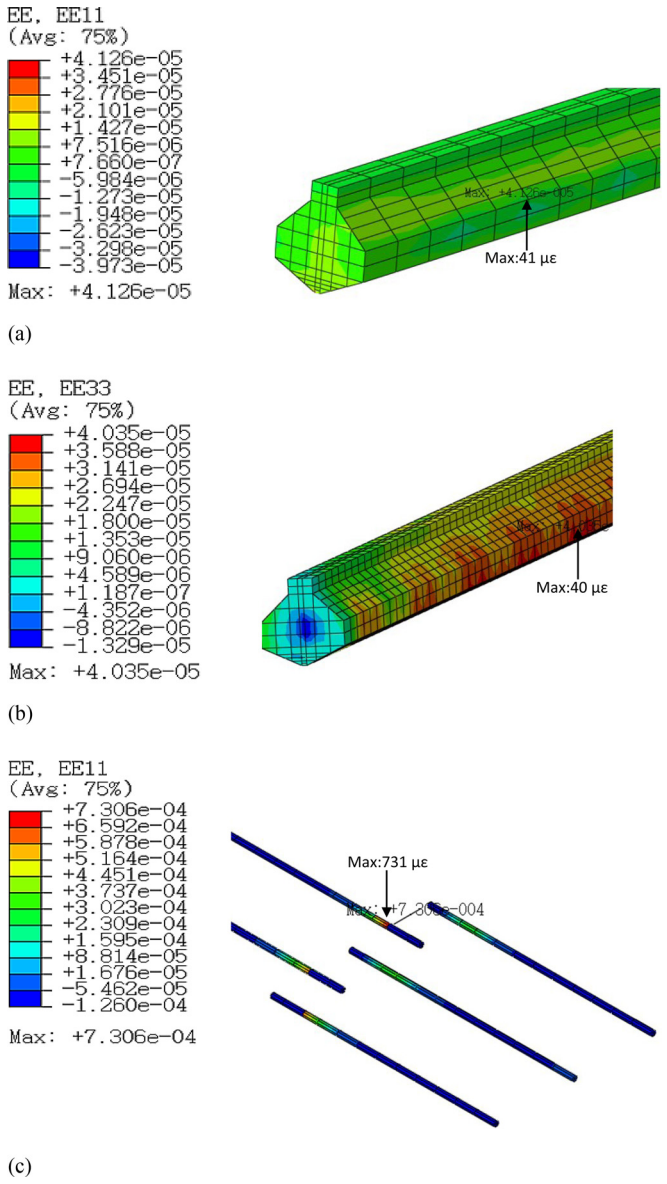

Fig. 12. Strain in shear keys and in dowel bars based on FE model for data on January 8, 2015 at 1200: (a) transverse strain in shear key; (b) longitudinal strain in shear key; and (c) axial strain in dowel bars.

at 50.8 mm from the interface for the portion embedded in the beams and at 38.1 mm from the interface for the portion embedded in the shear keys. Furthermore, the instrumented dowel bars were at the mid- and quarter-spans only. The observed strain in the dowel was near the support. This strain needs further investigation because it may be related to the restraint of the support and/or the dowel tried to prevent the opening and closing of the joints near the support, which created a high tensile strain in the dowel.

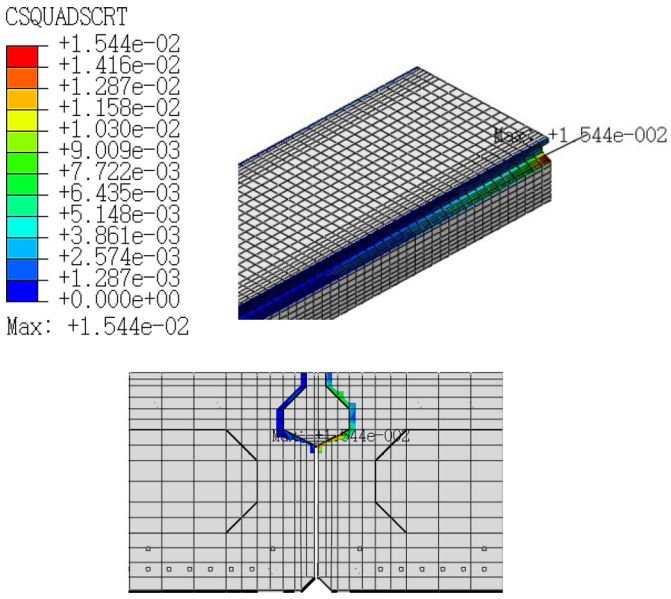

Fig. 13. DI for temperature distribution on January 8, 2015 at 1200.

The damage index (DI) of the interface bond was also investigated based on the FE model, as presented in Fig. 13. The DI is a measure of the degradation and eventual failure of the bond at the beam–key interface. This value from the FE model was calculated from Eq. (4), which represents the ratio between the calculated stresses and the allowable stresses at the interface. The lowest DI was observed on January 7, 2015 at 2100, which was only 0.0174%. This observation was consistent with the low transverse tensile strain in the shear keys and low axial tensile strain in the dowel bars. The DI at the interface bond increased as the transverse strain increased. The maximum DI at the interface was 1.5% and was observed on January 8, 2015 at 1200, which indicates that this temperature distribution gradient (the top flange and web temperature gradients were lower than the temperature gradient in the bottom flange) had more effects on the interface bond at the beam–shear key interface. The DI developed due to change in temperature for a specific time period. The DI was also concentrated near the support, which indicates the possibility that the interface failure started at the support and propagated toward the midspan. The interface failure will occur when the normal stress ratio equals unity. However, no damage was anticipated to occur under the temperature level that was considered.

Conclusions and Recommendations

The effects of different temperature distributions on the thermally induced stresses in UHPC shear key connections were investigated.

Downloaded from ascelibrary.org by Iowa State University on 01/28/19. Copyright ASCE. For personal use only; all rights reserved.

Based on the findings from this study, the following conclusions were drawn:

- The measured positive and negative temperature gradients corresponded with the temperature gradient from AASHTO (2016). However, the measured temperature gradient was slightly lower than the AASHTO LRFD design specifications.
- The bridge average temperature was in the range of the Ohio maximum and minimum temperatures. This indicates that the AASHTO LRFD range is extremely high and is conservative when used in the design of box beam bridges with and without UHPC shear key connections.
- The largest field strain in shear key connections was observed when the temperature gradient changed from negative to positive gradient. The beams' top flange and web temperature gradients were lower than the temperature gradient in the bottom flange. This temperature gradient is not considered in the current AASHTO LRFD bridge design specifications, although it produced the highest tensile strain in the UHPC connections.
- The longitudinal tensile strain in the UHPC shear key was much higher than the value in the beams, although the gauges were located at the same height. This difference in the strain created high shear stress at the beam–shear key interfaces.
- The maximum observed tensile strain from almost all instrumentation in the transverse direction occurred when the top flange and web of the beam were under negative temperature gradients and the bottom flange of the beam was under a positive temperature gradient. This indicates that this temperature gradient had more effects on the behavior of the bridge and UHPC shear key connections.
- The FE model was validated under different temperature distributions and showed the ability to capture the behavior of the bridge by comparing well with the field data. However, the observed high tensile strain in the dowel bars near the supports based on the FE model needs more investigation. The dowel bars near the supports were not instrumented and should be in the future to justify this observation.
- The lowest DI at the interface bond was observed on January 7, 2015 at 2100, which was only 0.0174%. This observation was consistent with the low transverse strain that was observed in the shear keys and low axial strain in the dowel bars. The DI at the interface increased as the transverse strain increased. The maximum DI at the interface bond was 1.5% and was observed on January 8, 2015 at 1200 and at 1800, which indicates that these temperature gradients had more effects on the interface bond at beam–shear key interfaces.

The maximum transverse tensile strain in UHPC shear key connections occurred when the temperature gradients in the top and web were negative and the temperature gradient in the bottom was positive. This observed temperature gradient should be considered in AASHTO LRFD bridge design specifications for adjacent box beam bridges.

Acknowledgments

The research team extend their gratitude to Steve Luebbe, the Fayette County engineer; Tim Keller, of the Office of Structural Engineering at the Ohio Department of Transportation for the project; Benjamin Graybeal of the Turner-Fairbank Highway Research Center, Federal Highway Administration; Luke Dlugosz and Kyle Nachuk of LaFarge North America and Vic Perry of V.iConsult, Inc. (formerly of LaFarge North America); Robert Ballard and Rob Cunningham from United Research Services (URS); and the bridge general contractor, the Righter Company, Inc., from Columbus, Ohio.

Notation

The following symbols are used in this paper:

A_i = area of the beam cross section of ith segment;
E_i = modulus of elasticity of the cross section of ith segment;
T_{avg} = average of the beam temperature over beam cross section;
T_i = temperature of the cross section of ith segment; and
α_i = coefficient of the thermal expansion of the material used for the ith segment.

References

Aaleti, S., H. Honarvar, S. Sritharan, M. Rouse, and T. Wipf. 2014. *Structural Characterization of UHPC waffle bridge deck and connections*. IHRB Project TR-614. Ames, IA: Bridge Engineering Center Iowa State Univ.

AASHTO. 2004. *LRFD bridge design specifications.* 3rd ed. Washington, DC: AASHTO.

AASHTO. 2016. *LRFD bridge design specifications.* 6th ed. Washington, DC: AASHTO.

ACI (American Concrete Institute). 2014. *Building code requirements for structural concrete*. ACI 318-14. Farmington Hills, MI: ACI.

ASTM. 2003. *Standard test method for bond strength of adhesive systems used with concrete as measured by direct tension*. ASTM C1404/C1404M-98. West Conshohocken, PA: ASTM.

Dong, X. 2002. "Traffic forces and temperature effects on shear key connections for adjacent box girder bridge." Doctoral dissertation, Univ. of Cincinnati.

Grace, N. F., E. A. Jensen, and M. R. Bebawy. 2012. "Transverse post-tensioning arrangement for side-by-side box-beam bridges." *PCI J.* 57 (2): 48–63. https://doi.org/10.15554/pcij.03012012.48.63.

Graybeal, B., I. De la Varga, and Z. Haber. 2017. *Bond of field-cast grouts to precast concrete elements*. FHWA-HRT-16-081. Washington, DC: Federal Highway Administration.

Hedegaard, B., C. French, and C. Shield. 2013. "Investigation of thermal gradient effects in the I-35W St. Anthony Falls bridge." *J. Bridge Eng.* 18 (9): 890–900. https://doi.org/10.1061/(ASCE)BE.1943-5592.0000438.

Imbsen, R. A., D. E. Vandershaf, R. A. Schamber, and R. V. Nutt. 1985. *Thermal effects in concrete bridge superstructures*, 12–22. DC.NCHRP Project. Rep. Washington, DC: Transportation Research Board.

Kong, B., C. S. Cai, and F. Pan. 2014. "Thermal field distributions of girder bridges with GFRP panel deck versus concrete deck." *J. Bridge Eng.* 19 (11): 04014046. https://doi.org/10.1061/(ASCE)BE.1943-5592.0000617.

Mahama, F., D. C. Walter, N. Currier, H. R. Hamilton, and G. R. Consolazio. 2009. *Validation of stresses caused by thermal gradient in segmental concrete construction*. Rep. 00030906. Gainesville, FL: Univ. of Florida.

Miller, R. A., G. M. Hlavacs, T. Long, and A. Greuel. 1999. "Full-scale testing of shear keys for adjacent box girder bridges." *PCI J.* 44 (6): 80–90. https://doi.org/10.15554/pcij.11011999.80.90.

Perry, V. H., and M. Royce. 2010. "Innovative field-cast UHPC joints for precast bridge decks (side-by-side deck bulb-tees), Village of Lyons, New York: Design, prototyping, testing and construction." *3rd fib Int. Congress*. Washington, DC: Federal Highway Administration.

Phares, B., J. M. Rouse, and J. Miksell. 2013. *Laboratory and field testing of an accelerated bridge construction demonstration bridge: US Highway 6 bridge over Keg Creek*. Trans. Project 11-411. Ames, IA: Bridge Engineering Center, Iowa State Univ.

Potgieter, I. C., and W. L. Gamble. 1983. "Response of highway bridges to nonlinear temperature distributions." Rep. FHWA/IL/UI-201. Urbana-Champaign, IL: Univ. of Illinois at Urbana-Champaign.

Rodriguez, L., P. Barr, and M. Halling. 2014. "Temperature effects on a box-girder integral-abutment bridge." *J. Perform. Constr. Facil.*

Downloaded from ascelibrary.org by Iowa State University on 01/28/19. Copyright ASCE. For personal use only; all rights reserved.

28 (3): 583–591. https://doi.org/10.1061/(ASCE)CF.1943-5509.0000437.
Royce, M. 2016. "Utilization of ultra high performance concrete (UHPC) in New York." In *First Int. Interactive Symp. on UHPC*. Des Moines, IA: Iowa State Univ.
Russell, H., and B. Graybeal. 2013. *Ultra-high performance concrete: A state-of the-art report for the bridge community*, 171. FHWA-HRT-13-060. Washington, DC: US Dept. of Transportation, Federal Highway Administration.
Semendary, A., E. Steinberg, K. Walsh, and E. Barnard. 2017a. "Live-load moment-distribution factors for an adjacent precast prestressed concrete box beam bridge with reinforced UHPC shear key connections." *J. Bridge Eng.* 22 (11): 04017088. https://doi.org/10.1061/(ASCE)BE.1943-5592.0001127.
Semendary, A., K. Walsh, and E. Steinberg. 2017b. "Early-age behavior of an adjacent prestressed concrete box-beam bridge containing UHPC shear keys with transverse dowels." *J. Bridge Eng.* 22 (5): 04017007. https://doi.org/10.1061/(ASCE)BE.1943-5592.0001034.
Steinberg, E., A. Semendary, and K. Walsh. 2015. "Adjacent precast box-beam bridges using UHPC longitudinal joints." *Constr. Specifier* 68 (8): 28–42.
Yuan, J., and B. Graybeal. 2014. *Bond behavior of reinforcing steel in ultra-high performance concrete*. FHWA-HRT-14-090. Washington, DC: US Dept. of Transportation, Federal Highway Administration.
Yuan, J., and B. Graybeal. 2016. "Full-scale testing of shear key details for precast concrete box-beam bridges." *J. Bridge Eng.* 21 (9): 04016043. https://doi.org/10.1061/(ASCE)BE.1943-5592.0000906.

Downloaded from ascelibrary.org by Iowa State University on 01/28/19. Copyright ASCE. For personal use only; all rights reserved.